

Mg/Ca ratios in freshwater microbial carbonates: Thermodynamic, Kinetic and Vital Effects.

P. Saunders^a, M. Rogerson^{a*}, J.D. Wadhawan^b, G. Greenway^b, H.M. Pedley^a

^a Department of Geography, Environment and Earth Science, University of Hull, Cottingham Road, Hull, HU6 7RX, UK.

^b Department of Chemistry, University of Hull, Cottingham Road, Hull, HU6 7RX, UK.

* Corresponding author: m.rogerson@hull.ac.uk

Abstract

The ratio of magnesium to calcium (Mg/Ca) in carbonate minerals in an abiotic setting is conventionally assumed to be predominantly controlled by $(\text{Mg}/\text{Ca})_{\text{solution}}$ and a temperature dependant partition coefficient. This temperature dependence suggests that both marine (e.g. foraminiferal calcite and corals) and freshwater (e.g. speleothems and surface freshwater deposits, “tufas”) carbonate deposits may be important archives of palaeotemperature data. However, there is considerable uncertainty in all these settings. In surface freshwater deposits this uncertainty is focussed on the influence of microbial biofilms. Biogenic or “vital” effects may arise from microbial metabolic activity and / or the presence of extracellular polymeric substances (EPS). This study addresses this key question for the first time, via a series of unique through-flow microcosm and agitated flask experiments where freshwater calcite was precipitated under controlled conditions. These experiments reveal there is no strong relationship between $(\text{Mg}/\text{Ca})_{\text{calcite}}$ and temperature, so the assumption of thermodynamic fractionation is not viable. However, there is a pronounced influence on $(\text{Mg}/\text{Ca})_{\text{calcite}}$ from precipitation rate, so that rapidly forming precipitates develop with very low magnesium content indicating kinetic control on fractionation. Calcite precipitation rate in these experiments (where the solution is only moderately supersaturated) is controlled by biofilm growth rate, but occurs even when light is excluded indicating that photosynthetic influences are not important. Our results thus suggest the apparent kinetic fractionation arises from the electrochemical activity of EPS molecules, and are therefore likely to occur wherever these molecules occur, including stromatolites, soil and lake carbonates and (via colloidal EPS) speleothems.

1. Introduction

The potential of the $(\text{Mg}/\text{Ca})_{\text{calcite}}$ palaeothermometer was first observed in the 1950’s when a link between latitude and magnesium content was recognised in a study on the

33 biogeochemistry of marine skeletal calcites (Chave, 1954). The use of $(\text{Mg}/\text{Ca})_{\text{calcite}}$ ratios as
 34 a palaeothermometer has since become widespread in marine settings with many studies on
 35 benthic and planktonic foraminifera (Delaney *et al.*, 1985, Nurnberg *et al.*, 1996, Rosenthal *et al.*,
 36 *et al.*, 1997, Anand *et al.*, 2003, Elderfield *et al.*, 2006, Kisakurek *et al.*, 2008, Boussetta *et al.*,
 37 2011, Martinez-Boti *et al.*, 2011) and to a lesser extent in corals (Mitsuguchi *et al.*, 1996,
 38 Shirai *et al.*, 2005, Wei *et al.*, 2000; Yu *et al.*, 2005, Reynaud *et al.*, 2007). Surface
 39 freshwater carbonates (“tufa”) are ambient temperature freshwater deposits which have been
 40 considered, but not thoroughly investigated, as potential archives of terrestrial
 41 palaeotemperature data through their Mg/Ca ratios (Garnett *et al.*, 2004; Rogerson *et al.*,
 42 2008, Brasier *et al.*, 2010, Lojen *et al.*, 2009).

43 A number of divalent cations are able to substitute for the position of Ca^{2+} in the calcite
 44 crystal structure. The degree to which this substitution occurs is generally expressed through
 45 a partition coefficient (K_d). The heterogeneous partition coefficient for the partitioning of
 46 Mg^{2+} between a carbonate mineral and the aqueous solution is given by the equation (Oomori
 47 *et al.*, 1987):

$$48 \log \frac{(m_{\text{Mg}^{2+}})_i}{(m_{\text{Mg}^{2+}})_f} = \lambda_{\text{Mg}} \frac{(m_{\text{Ca}^{2+}})_i}{(m_{\text{Ca}^{2+}})_f}$$

49 Where m is the concentration of the subscripted species and i and f represent the initial and
 50 final solutions respectively. In the carbonate literature the partition coefficient is usually
 51 expressed in the general simple form:

$$52 K_d = \frac{(Tr/Ca)_{\text{CaCO}_3}}{(Tr/Ca)_{\text{soln}}}$$

53 Where Tr is the trace cation and K_d is the partition coefficient. Mg/Ca palaeothermometry
 54 therefore relies on the thermodynamic control of the partitioning of trace elements in the
 55 carbonate crystal lattice being sufficiently dominant from other effects so as to reduce them
 56 to “noise”. Studies on inorganic calcite have confirmed that, under controlled conditions, the
 57 dominant control on Mg partitioning in carbonates is indeed temperature, with other factors
 58 such as precipitation rate having little influence (Mucci, 1987, Morse and Bender, 1990).
 59 However, evidence from natural (i.e. non-controlled) conditions shows the value of K_d to be
 60 dependent on significant complicating factors arising from precipitation rate, crystal

61 morphology and spatially / temporally variable solution composition (Fairchild and Treble,
62 2009).

63 **1.1 Mg/Ca in Tufa carbonates and the conjectured role of Extracellular** 64 **Polymeric Substances.**

65 To date very few studies have had any real focus on utilising tufa (Mg/Ca)_{calcite} ratios as a
66 palaeothermometer. Incorporation of Mg²⁺ into tufas deposited in the summer was found to
67 be higher than in winter (Chafetz *et al.*, 1991) and a seasonal temperature change in stream
68 water of ~ 10 °C appeared to be the dominating influence on Mg²⁺ incorporation into a 14
69 year (1985 – 1999) tufa record from Queensland Australia, although there were considerable
70 discrepancies in the correlation between the tufa (Mg/Ca)_{calcite} ratios and water temperature
71 (Ihlenfeld *et al.*, 2003). Although these studies show support for the potential of tufa
72 (Mg/Ca)_{calcite} palaeothermometry they do not take into account the presence of microbial
73 biofilms and the significant impact they may have on trace element incorporation into tufa
74 carbonates. The discrepancies observed by Ihlenfeld *et al.*, (2003) may be due to the presence
75 of a spatially inconsistent and heterogeneous microbial biofilm with its associated
76 metabolism and/or the chemoselective chelation of cations from the river water by EPS
77 molecules.

78 Unlike corals and foraminifera, where all precipitation is biogenic (Elderfield *et al.*, 1996,
79 Yoshimura *et al.*, 2011) and speleothems where precipitation is usually assumed to be
80 abiogenic (although biogenic precipitation has been demonstrated, e.g. (Cacchio *et al.*,
81 2004), the role of biology in determining tufa carbonate chemistry is poorly understood
82 (Pedley *et al.*, 2009). Recent research efforts have been focussed on the impact of the
83 presence of extracellular polymeric substances (EPS), which have the capacity to be a first-
84 order control on the precipitation chemistry (Dittrich *et al.*, 2003, Bissett *et al.*, 2008). EPS
85 has demonstrated the ability to bind divalent cations, resulting from the fact that most EPS
86 molecules have negatively charged functional groups which deprotonate as pH increases
87 (Konhauser, 2007, Dittrich and Sibling, 2010). Studies on cyanobacteria and sulphate reducing
88 bacteria (SRB) have revealed that the functional groups include carboxylic acids (R-COOH),
89 hydroxyl groups (R-OH), amino groups (R-NH₂), sulphate (R-O-SO₃H), sulphonate (R-
90 SO₃H), and sulphhydryl groups (-SH), all of which bind metal ions including Ca²⁺ and Mg²⁺
91 (Dupraz *et al.*, 2009 and references therein). It has been demonstrated that chelation strongly
92 favour ions with low charge density thus favouring Ca²⁺ over Mg²⁺ (Rogerson *et al.*, 2008).

93 This influence could be transmitted to solid carbonate chemistry by altering the M^{2+} / Ca^{2+}
94 ratios within the biofilm interstitial waters from which carbonates are precipitated and also by
95 directly influencing the precipitation mechanism itself. Variations in trace element chemistry
96 within hyper-alkaline lacustrine carbonate have recently been identified, with high calcium
97 carbonates presented in close proximity to cells (Couradeau et al., 2013). However, the direct
98 link to EPS intermediary states remains untested.

99 The primary mechanism by which EPS electroselectivity can be transmitted to precipitates
100 arises from the fact that chelation of ions is not a permanent state, ions constantly move
101 between bound states and solution. The ratio of ions in the solution in the immediate vicinity
102 of the chelation sites is consequently determined by the binding preferences of the EPS. As
103 Ca^{2+} is selectively favoured over Mg^{2+} by EPS molecules then the $(Mg/Ca)_{solution}$ in this
104 environment will be reduced relative to the bulk water. Therefore, calcite precipitation
105 initiated on a calcite surface covered in biofilm will occur at the nucleation sites enriched
106 with calcium ions relative to magnesium. Any precipitates forming in the immediate
107 environment of the EPS will therefore have a $(Mg/Ca)_{calcite}$ lower than would be expected
108 given the bulk water $(Mg/Ca)_{solution}$.

109 The generation of low $(Mg/Ca)_{calcite}$ within the EPS matrix will be accentuated by the low
110 Mg^{2+} concentrations in this microenvironment. It has been demonstrated that calcite
111 precipitation rates are reduced in the presence of Mg^{2+} (Morse and Mackenzie, 1990,
112 Paquette *et al.*, 1996, Zhang and Dawe, 2000) and that this reduction is approximately
113 proportional to the $(Mg/Ca)_{solution}$ (Morse and Mackenzie, 1990, Zhang and Dawe, 2000).
114 Therefore the lower $(Mg/Ca)_{solution}$ in the immediate microenvironment of the EPS molecules
115 created by the chemoselectivity for Ca^{2+} will result in a faster precipitation rate in these
116 regions of the biofilm compared to other areas where the $(Mg/Ca)_{solution}$ is greater. This effect
117 will become cumulative at higher precipitation rates, driving down the mean $(Mg/Ca)_{calcite}$ of
118 precipitates generated within the biofilm.

119 This study tests the hypothesis that the presence of biofilm results in precipitation of reduced
120 $Mg/Ca_{(calcite)}$ for the first time, and also tests whether this effect is sufficient to suppress
121 classic thermodynamic controls for the first time.

122 2. Methods

123 2.1 Experimental design

124 The microcosm system was based on the recirculating flume system developed at the
125 University of Hull (Rogerson et al., 2010, Pedley et al., 2009). It was designed to allow the
126 flow through of experimental water through a series of four identical micro-flumes. The
127 design is shown in Figure 1 (which also includes the experimental design of the additional
128 conical flask experiments (see section 2.4)). The apparatus was housed in a windowless, air
129 conditioned laboratory where the ambient laboratory air temperature was maintained between
130 16 and 20 °C by an ‘Airforce Climate Control’ air conditioning unit (10,000 BTU hr⁻¹; 2.9
131 kW cooling capacity, Airconwarehouse, Stockport, UK). This provided the experiments some
132 buffering from variations in room temperatures due to seasonal and diurnal changes.
133 Experiments were performed for a period of 28 days and consisted of four replicates which
134 were run within identical Perspex micro-flumes with dimensions of 20 cm by 8 cm and a
135 depth of 2.5 cm. Each flume was constructed with a 7 mm wide flow channel with a Perspex
136 lid providing a water tight seal. For the duration of the experimental runs the flumes were
137 submerged in a metallic water bath to ensure tight control on precipitation temperature.
138 Experiments were conducted at 12 ± 0.2, 14 ± 0.2, 16 ± 0.2, 18 ± 0.2 and 20 ± 0.5 °C
139 (Saunders *et al.*, in press).

140 The water bath temperature was controlled via a Titan 150 mini cooler chiller unit (Aqua
141 Medic, Bisendorf, Germany). Water was re-circulated through the chiller unit via a submerged
142 pump in the sump and the bath itself was surrounded by sheets of thermal aluminium foil
143 (thermal resistance 1.455 m² K W⁻¹) to provide additional thermal buffering and exclude
144 incoming UV from the water bath. Only the micro-flumes were left exposed to the lighting
145 unit to allow photosynthesis. Sheets of thermal aluminium foil were placed over piping which
146 was external to the water bath to prevent heating from the lighting unit. The chiller unit was
147 able to provide temperature control at 12, 14, 16 and 18 °C. The unit was unable to maintain
148 the water temperature at 20 °C so additional heating was provided by a thermostatically
149 controlled Aqua One 100 W fully submersible aquarium heater (Aqua Pacific Ltd.,
150 Southampton, UK) placed in the sump. The temperature of the water bath was monitored at
151 ten minute intervals via a calibrated thermometer probe (range -50 to 200 °C) (Thermometers
152 Direct, Aldershot, UK) inserted next to the microcosms. The digital output from the
153 thermometer was recorded to a PC via a webcam system, so each experiment is represented

154 by over 4000 individual recorded water temperature measurements. Photosynthetic light was
155 supplied to the system via a single ‘Thorn Lopak 250 W HPS-T’ sodium lamp on a 7 hour on
156 and 17 hour off cycle to avoid excessive light incidence, which previous experiments had
157 demonstrated bleached the biofilm.

158

159 **2.2 Biofilm**

160 Biofilm was sourced from the River Lathkill, Derbyshire (UK grid reference SK 225 645).
161 Initial colonisation was onto carbon fabric secured to house bricks which were submerged in
162 an active tufa precipitating reach on the 3rd of April 2009 and recovered on the 5th of August
163 2009. To ensure a constant supply of a common biofilm, which was free of “inheritance”
164 calcite, the colonised carbon fabric was detached from the bricks and secured within a 1
165 metre long, 112 mm wide polycarbonate gutter within a mesocosm (see Rogerson et al., 2009
166 and Pedley et al., 2009). 30 L of deionised (15 M Ω) water was circulated between the
167 colonising gutter and a sump via a Titan 150 in line chiller set at 12 °C. The colonising flume
168 was illuminated by a single ‘Thorn Lopak 250 W HPS-T’ hydroponic lamp on a 7 hour on
169 and 17 hour off cycle. This “colonisation” flume was used to colonise clean plastic mesh
170 pads, after which the source biofilm was removed and the water replaced with fresh, 15 M Ω
171 water. The colonisation process was continued for a further 3 months to achieve a sustainable
172 amount of completely sediment-free and carbonate-free biofilm for all future experiments. To
173 avoid nutritional deprivation a 30 ml dose of an organic liquid was added at monthly
174 intervals. The organic liquid was obtained from the decomposition of tree leaves from Welton
175 Beck catchment (water source for the colonising flume). This nutritional regime had proved
176 successful in previous experiments within the same laboratory (see Pedley *et al.*, 2009), and
177 minimises the change in the balance of diatoms and cyanobacteria inevitable once a biofilm
178 body is removed from its natural environment.

179 Prior to the first experiment a sample of the newly colonised biofilm was taken and prepared
180 for examination by scanning electron microscopy (SEM). No calcite precipitates could be
181 observed, and the culture visually resembled the source biofilm in terms of its biological
182 composition.. Ecologically, the biofilms comprised a mixed diatom and cyanobacterial mat
183 associated with a variety of bacterial taxa not possible to identify visually. EPS found in
184 cultured films were similar in appearance and density as those found in the field.
185 Experimental biofilm was recovered via standard glass microscope slides cut to 5 mm wide

186 strips and frosted with corundum glass frosting powder which were secured to the colonised
187 mesh pads and could be removed and imported into the micro-flumes immediately and
188 without further alteration.

189 **2.1 Trace element analysis**

190 All water chemistry analyses was undertaken on a Perkin Elmer Optima 5300DV (Perkins-
191 Elmer, Waltham, MA, USA) inductively coupled optical emission spectrometer (ICP – OES).
192 The selection of the analytical lines used in the results was based on the Perkin Elmer
193 recommendations for the Optima 5300 DV spectrometer, 393.366 nm for calcium and
194 280.271 nm for magnesium. Calibration standards were prepared using 1000 ppm standard
195 stock solutions (99.9% pure or greater, PrimAg, Xtra, Romil, Cambridge) of calcium and
196 magnesium. Mixed standards of calcium and magnesium were prepared through dilution with
197 2% ultrapure HNO₃ to give calibration standards of 1, 2, 3, 4 and 5 ppm for calcium and 0.1,
198 0.2, 0.3, 0.4, and 0.5 ppm for magnesium. Samples for analysis were diluted with 5 %
199 ultrapure HNO₃ to bring the expected concentrations to within or very near the linear
200 calibration of the standards.

201 **2.2 Experimental solution**

202 Initial water for the experiments was collected from a spring sourced by a Cretaceous chalk
203 aquifer at Welton Beck, East Yorkshire (UK grid reference SE 965 275). Although there were
204 variations in springwater chemistry, the concentrations of Mg²⁺_(aq) and Ca²⁺_(aq) in the spring
205 water were fairly stable ranging from 2.6 – 5.1 mg L⁻¹ for magnesium and 82.9 – 141.2 mg L⁻¹
206 for calcium. To ensure the water for all experiments had equal levels of Mg²⁺_(aq) and Ca²⁺_(aq)
207 acetates of calcium (Ca(C₂H₃O₂)₂) and magnesium (Mg(C₂H₃O₂)₂) (Alfa Aesar,
208 Massachusetts., USA) were added to the spring water to bring the concentrations of Mg²⁺_(aq)
209 and Ca²⁺_(aq) to 8.0 and 160 mg L⁻¹ respectively giving a constant (Mg/Ca)_{solution} molar ratio
210 of 0.082. The pH of the source water was rather invariable at 8.2 ± 0.2, and bicarbonate
211 alkalinity 180 ± 22 mg L⁻¹. The solution was analysed before and after addition to ensure
212 minimum variance in this composition, and therefore changes in solution chemistry
213 throughout the experiments described herein are negligible. Acetates were used to avoid
214 contaminating the solution with variable levels of exotic counter-ions; organic acids were
215 already present in high concentrations in the dissolved components of the EPS and
216 considered the most “inoffensive” counter ion in our context. The saturation state was

217 determined using the aqueous geochemical modelling software PHREEQC. Saturation index
218 values for the experimental solutions were 0.95, 0.98, 1.01, 1.04 and 1.07 for the
219 temperatures, 12, 14, 16, 18 and 20 °C respectively

220 **2.3 Precipitate recovery**

221 At the end of each experiment the glass slides containing the biofilm and experimental
222 precipitates were removed from the microcosms and the biofilm covering of the glass slide
223 was added to 20 mL sterilin tubes and centrifuged in a Centaur 2 non refrigerated bench top
224 centrifuge (MSE, London, UK) at 3300 rpm for 20 minutes. The supernatant water was
225 discarded. Prior to dissolution of the calcite precipitates in the biofilm it was necessary to
226 'clean' the biofilm of Mg^{2+} and Ca^{2+} cations that had been chelated by the EPS of the biofilm
227 complex. Ultrapure water (18 M Ω) was added to each tube containing the biofilm pellet. The
228 tube was shaken vigorously to ensure full mixing of the biofilm with the water and left to
229 stand for two hours. It was then centrifuged at 3500 rpm for 15 minutes. A sample was taken
230 of the supernatant and immediately acidified with 5 % ultrapure HNO_3 for analysis of the
231 $Mg^{2+}_{(aq)}$ and $Ca^{2+}_{(aq)}$ levels by ICP – OES. This process was repeated five or six times to
232 ensure all practical chelated Mg^{2+} and Ca^{2+} cations were washed from the biofilm (as
233 confirmed by ICP – OES analyses). The biofilm pellet was then oven dried. The dissolution
234 of calcite precipitates held within the dried biofilm pellet was achieved by gravimetrically
235 adding 10% ultrapure HNO_3 to the sample. The samples were sonicated for three minutes in
236 an Ultra 8000 bench top ultrasonic cleaner (Ultrawave, Cardiff, UK) left to stand for two
237 hours, shaken vigorously, sonicated again and centrifuged for 15 minutes at 3300 rpm. A
238 sample of the supernatant was taken and immediately acidified with ultrapure 5 % HNO_3 for
239 analysis of $Mg^{2+}_{(aq)}$ and $Ca^{2+}_{(aq)}$ levels and determination of the precipitate $(Mg/Ca)_{calcite}$
240 ratios.

241 **2.4 Additional experiments**

242 Additional experiments were conducted in 150 ml conical flasks. Experiments were
243 conducted at 12 ± 0.5 , 14 ± 0.2 , 16 ± 0.3 , 18 ± 0.2 and 20 ± 0.5 °C. The flasks were secured
244 to a Stuart SF1 flask shaker (Bibby Scientific Limited, Staffordshire, UK) which was set to
245 100 oscillations per minute for all experiments to promote oxygenation of the solutions.

246 Eight 150 mL conical flasks were used with two replicates each of three different treatments
247 and two controls. The treatments consisted of biofilm exposed to solar spectrum light (BFL)

248 and biofilm with light excluded (BFD). The biofilm used was taken from the same colonising
249 flume as the microcosm experiments. Each flask for the biofilm treatments received 3 g of
250 biofilm and 50 mL of prepared solution. The two flasks from which light was excluded were
251 thoroughly wrapped in reflective thermal aluminium foil (thermal resistance $1.455 \text{ m}^2 \text{ K W}^{-1}$)
252 to exclude all light. Foam bungs were used to prevent microbial invasion and reduce
253 evaporative loss from the flasks whilst allowing gas exchange. The flasks were clamped to
254 the shaker and further thermal aluminium foil (thermal resistance $1.455 \text{ m}^2 \text{ K W}^{-1}$) was used
255 to cover the sections of the water tank containing the light excluded replicates. Solution
256 preparation, the removal of chelated cations and precipitate recovery followed the procedures
257 described for the microcosm experiments.

258 **3. Results**

259 **3.1 $(\text{Mg}/\text{Ca})_{\text{calcite}}$ and precipitation temperature**

260 Binary plots of $(\text{Mg}/\text{Ca})_{\text{calcite}}$ ratios and temperature for the microcosm and agitated flask
261 experiments are shown in Figure 2. In all cases, control data (where precipitation is solely
262 physical) shows a positive correlation to temperature, approximately conforming to the
263 expected exponential correlation with $\text{Mg}/\text{Ca} = 0.0029e^{0.1568T}$ ($R^2 = 0.90$, $P < 0.05$).
264 However, the microcosm data (Fig 2 (a)) does not conform to the expected relationship,
265 instead it reveals a weak negative linear correlation between Mg/Ca and temperature in the
266 presence of biofilm ($P < 0.05$, $R^2 = 0.44$) so that $(\text{Mg}/\text{Ca})_{\text{calcite}}$ generally decreases as
267 temperature increases. Apart from the $20 \text{ }^\circ\text{C}$ experiment there is considerable variation of
268 $(\text{Mg}/\text{Ca})_{\text{calcite}}$ ratios at a given temperature; at $14 \text{ }^\circ\text{C}$ there is nearly an order of magnitude
269 range. The flask experiment data for both BFL and BFD follow an almost identical pattern to
270 that of the microcosm data (Fig. 2 (b & c)), although again with considerable scatter. Two
271 replicates have plots well off the general pattern; both are at $18 \text{ }^\circ\text{C}$, one from the BFL and
272 one from the BFD. The presence of the potentially anomalous data points at $18 \text{ }^\circ\text{C}$ results in
273 no significant correlation between temperature and $(\text{Mg}/\text{Ca})_{\text{calcite}}$ for the BFL or BFD
274 experiments ($R^2 = 0.13$, and $R^2 = 0.16$ respectively). The exclusion of the anomalous data
275 points results in a significant negative power relationship at the 95 % confidence level for
276 both BFL ($R^2 = 0.76$) and BFD experiments ($R^2 = 0.88$) respectively. Combining the data
277 generated from the microcosm and agitated flask experiments (Fig. 2 (d) gives no correlation
278 between $(\text{Mg}/\text{Ca})_{\text{calcite}}$ and temperature for precipitates generated in the presence of biofilm.

279 **3.2 Temperature and precipitation rate**

280 Binary plots of precipitation rates and temperature are presented in Figure 3. The microcosm
281 data (Fig 3 (a)) present a significant ($P < 0.05$) exponential correlation ($R^2 = 0.86$). No
282 significant correlation was found between precipitation rate and temperature for BFL
283 precipitates (Fig 3 (b)) as data at 18 °C do not follow the general trend of increasing rate at
284 higher temperatures observed at the other temperatures (excluding these points reveals a
285 linear correlation; $P < 0.05$, $R^2 = 0.70$). The BFD precipitates (Fig. 3 (c)) reveal a linear
286 correlation significant at the 95 % confidence level ($R^2 = 0.48$). The strength of this
287 correlation is again reduced by the apparently anomalous data point at 18 °C, and removing
288 this data point again strengthens the correlation ($R^2 = 0.74$). Combining the data from the
289 microcosm and agitated flask experiments (Fig 3 (d)) results in an exponential relationship
290 between precipitation rate and temperature ($P < 0.05$, $R^2 = 0.45$).

291

292 **3.3 (Mg/Ca)_{calcite} and precipitation rate**

293 Figure 4 shows the relationship between (Mg/Ca)_{calcite} and precipitation rate. The control
294 data shows a significant linear correlation whereby (Mg/Ca)_{calcite} increases as precipitation
295 rates rise, which is consistent with theoretical expectations which predict that Mg²⁺
296 partitioning increases with increasing precipitation rate (Rimstidt *et al.*, 1998). In complete
297 contrast, the results from the microcosm experiments (Fig. 4 (a)) show a negative power
298 correlation between the parameters ($R^2 = 0.52$, $P < 0.05$) with (Mg/Ca)_{calcite} falling as
299 precipitation rates increases. Similarly, the relationship between the (Mg/Ca)_{calcite} ratios and
300 precipitation rate for the BFL and BFD experiments (Fig. 4 (b & c)) takes the form of a
301 negative power regression ($R^2 = 0.89$ and 0.83 respectively), and for both sets of data
302 combined ($R^2 = 0.79$) all of which are significant at the 95 % confidence level. Figure 4 (d)
303 plots the data from the microcosm, BFL and BFD experiments, the negative power
304 correlation observed individually in the experiments is still held ($P < 0.05$, $R^2 = 0.67$),
305 although there is a clear separation of the 20 °C data.

306 **4. Discussion**

307 **4.1 Precipitation temperature and (Mg/Ca)_{calcite}**

308 The experimental results reveal that the presence of a microbial biofilm overrides the
309 expected thermodynamic control on (Mg/Ca)_{calcite} in a freshwater environment, and that use

310 of tufa derived $(\text{Mg}/\text{Ca})_{\text{calcite}}$ as a palaeothermometer would be ill-advised. The data is not
311 random however, and the structure of relationships between the parameters clearly indicates
312 some form of significant microbial control. However, the coherent response of experiments in
313 the microcosms and flasks both in light and dark indicates that some other (non-
314 thermodynamic) controls are in operation. Other than at 20°C, the microcosm data show wide
315 variations in the $(\text{Mg}/\text{Ca})_{\text{calcite}}$ indicating that these controls are not simple. The agitated flask
316 experiments generally present a tighter relationship between $(\text{Mg}/\text{Ca})_{\text{calcite}}$ and temperature,
317 with the exception of two of the data points at 18 °C in both the BFL and BFD treatments.
318 Examination of all the original ICP – OES outputs do not reveal anything that may make
319 these values obviously erroneous, furthermore it cannot arise from some unexpected
320 ecological change as the systems are fundamentally dissimilar one being largely
321 heterotrophic and the other photosynthetic. The only common factor is that these flasks were
322 seeded with the same aliquot of biofilm, and it is possible that this aliquot had a significantly
323 different microbial or EPS composition which altered the behaviour of the biofilm in terms of
324 calcite precipitation.

325 **4.2 Temperature and calcite precipitation rate**

326 At a given saturation state, calcite precipitation should increase with increasing temperature
327 due to calcite solubility decreasing with increasing temperature (Morse and Mackenzie,
328 1990). Higher temperatures also increase precipitation rates through the increased kinetic
329 energy of the species, a higher number of collisions between ionic species at higher energies
330 will increase the likelihood of precipitation reactions overcoming the activation energy
331 barrier and going to completion. Increased calcification rates at higher temperatures have
332 been observed in laboratory experiments involving precipitation in the presence of bacterial
333 isolates (Cacchio *et al.*, 2003, Cacchio *et al.*, 2004, Baskar *et al.*, 2006), however, no studies
334 appear to have been conducted which examine precipitation rates as a function of temperature
335 in the presence of a full microbial biofilm.

336 We find no consistent relationship between the mean precipitation rates at a given
337 temperature (Table 1) and the precipitation environment (e.g. the flow-through microcosms
338 or the agitated flasks), but also no consistent differences between the three types of system
339 (microcosm, BFL and BFD). At the commencement of the experiments the Ω values were the
340 same for both microcosm and agitated flask experiments, and only marginally different
341 within the entire range of conditions ($\Omega = 0.95$ to 1.07), although in the agitated flasks there

342 was no replenishment of ions to the experimental solution so Ω values will have fallen over
343 time as precipitation took place. In the absence of other reasons to explain the breakdown of
344 the expected physicochemical behaviour, we again conclude that Mg/Ca_{calcite} is controlled by
345 microbial activity or the presence of EPS.

346 **4.3 $(Mg/Ca)_{\text{calcite}}$ and precipitation rate**

347 The negative power relationship between $(Mg/Ca)_{\text{calcite}}$ and precipitation rate derived from the
348 microcosm and agitated flask experiments is contradictory to theoretical expectations
349 suggesting that the presence of the biofilm has a strong influence on the correlation between
350 the parameters. Distribution coefficients (K) were calculated for both microcosm and agitated
351 flask precipitates using the standard equation $K = (Mg/Ca)_{\text{calcite}} / (Mg/Ca)_{\text{solution}}$ and are
352 presented as a function of precipitation rate in Figure 5 ($P < 0.05$, $R^2 = 0.67$). However,
353 empirical distribution coefficients differ from theoretical coefficients which are determined
354 from a system assumed to be at equilibrium. Experimental conditions can only approximate
355 equilibrium, furthermore kinetic effects result in non uniform trace element partitioning in
356 precipitates from actual experiments (Rimstidt *et al.*, 1998). For the purposes of the following
357 discussion empirical coefficients will be designated by (K_{em}) and equilibrium coefficients by
358 (K_{eq}). Table 2 shows the K_{em} K_{eq} and ionic radii for selected divalent cations. Experimental
359 evidence shows that a relationship exists between precipitation rates and K_{em} which is
360 dependent on the value of K_{eq} (Rimstidt *et al.*, 1998) where:

361 for elements with a $K_{eq} < 1$ (e.g. Mg^{2+}) the value of K_{em} is larger than K_{eq} and decreases
362 towards K_{eq} as precipitation rates fall.

363

364 for elements with $K_{eq} > 1$ the value of K_{em} is smaller than K_{eq} and increases towards K_{eq} as
365 precipitation rates fall.

366 These relationships have been observed experimentally (e.g. Lorens, 1981, Mucci 1987,
367 Pingitore *et al.*, 1988, Tesoriero and Pankow, 1996) in abiotic precipitates. Accordingly, at
368 faster precipitation rates the value of K_{em} for Mg^{2+} into calcite should increase as precipitation
369 rates rise. The K_{em} values obtained in the experiments described here are in complete contrast
370 to this and also to the K_{em} values obtained in experiments on inorganic calcite. Clearly,
371 normal chemical evolution of the solid from the solution is being prevented by the biofilm.

372 **4.4 The potential of biofilms to influence calcite precipitation chemistry**

373 The presence of a microbial biofilm in these experiments has shifted the $(\text{Mg}/\text{Ca})_{\text{calcite}}$ ratios
374 as a function of both temperature and precipitation rate away from theoretical expectations
375 but also from the type of relationships seen in other biogenic carbonates such as ostracodes,
376 foraminiferal and coral carbonate. This indicates that trace element ratios and precipitation
377 rates must be influenced by some aspect of the biofilm not present in other settings; these
378 must be specific microbial metabolic processes, structural components of the biofilm (EPS)
379 or a combination of both. Temperature variations have been shown to have an impact on
380 both biofilm microbial diversity and growth rates from photosynthesis and heterotrophic
381 metabolism within the temperature range of the experiments described here (Blanchard *et al.*,
382 1996, Watermann *et al.*, 1999, Defew *et al.*, 2004, Hancke and Glud, 2004, Salleh and
383 McMinn, 2011). The diversity of microorganisms held in a laboratory grown biofilm exposed
384 to specific light and temperature conditions is strongly dependant on species specific growth
385 rates and any species within the biofilm complex can only acclimatise to the imposed
386 environment within their individual genetic limits (Defew *et al.*, 2004). In
387 diatom/cyanobacterial biofilms such as those used in this work it has been observed that at 10
388 °C diatoms are the dominant organism but at 25 °C filamentous cyanobacteria dominate
389 (Watermann *et al.*, 1999). Others have observed that between 10 and 18 °C changes in
390 diatom species composition were minimal, but at 18 °C there was a significant change in the
391 species composition, with a significant shift to low diversity (Defew *et al.*, 2004). In light of
392 these observations it is assumed that over the range of 12 – 20 °C of the described
393 experiments considerable variation will have been induced in both genus and species
394 variations during the course of each experimental run.

395 Such changes in ecological structure will likely result in the changes in biogeochemical
396 behaviour found during our experiments. The finding of Waterman *et al.*, (1999) that
397 cyanobacteria are the dominant organisms in biofilms at higher temperatures may explain the
398 dramatic increase in precipitation rates at 20 °C seen in the microcosm experiments. Biofilm
399 microprofiles of pH, O₂, Ca²⁺ and CO₃²⁻ obtained by Shiraishi *et al.* (2008) showed that bright
400 green cyanobacteria dominated biofilms had a higher photosynthetic capacity and thus
401 exerted more influence on the carbonate system at the tufa surface. The enhanced creation of
402 an alkaline environment through the greater photosynthetic capacity of a cyanobacterial
403 dominated biofilm at 20 °C in the experiments described here may have enhanced
404 precipitation rates significantly over those at the lower temperatures where cyanobacteria
405 were not the dominant microorganism.

406 However, faster precipitation arising from ecological changes effect provides no mechanism
407 to provide the trend reversal in the Kr_{em} compared to the Kr_{eq} ; this requires first-order
408 alteration of the cationic biogeochemical system.

409 **4.4.1 Impact of EPS on $(Mg/Ca)_{calcite}$**

410 Involvement of a metal-organic phase at precipitation sites, which are actively exchanging
411 ions with ambient water (Rogerson et al, 2010), does provide a means of altering apparent
412 partition coefficients. The wide variations in $(Mg/Ca)_{calcite}$ ratios seen in the precipitates
413 generated within the biofilms of the microcosm experiments thus are likely to be a
414 consequence of heterogeneity in the composition of the functional groups within the biofilm
415 matrix.

416 Variations in species diversity have been shown to have a large impact on the composition
417 and amount of EPS produced (Di Pippo *et al.*, 2009), this is important given its ability to
418 chelate $Ca^{2+}_{(aq)}$ and $Mg^{2+}_{(aq)}$ from the bulk water of a calcite precipitating experimental
419 solution or natural system (Rogerson et al., 2008). The chelating ability of EPS molecules
420 depends on the availability of binding sites on negatively charged functional groups, which
421 may be reduced by interactions between EPS molecules by causing them to become sterically
422 inhibited or blocked (Dupraz *et al.*, 2009). The nature of these interactions will vary
423 alongside changes in biofilm composition. It has been suggested that the physical state of
424 EPS also influences the binding abilities, whereby EPS in a gel state may bind more strongly
425 with a particular cation than one in a loose slime state (Decho, 2000).

426 In addition to changes in binding abilities (i.e. the amount of a specific cation) there is a
427 further potential influence on $(Mg/Ca)_{calcite}$ arising from EPS through chemoselectivity,
428 especially as pervasive EPS has been found associated with carbonate precipitates down to
429 the nm scale (Benzerara et al., 2006). The favouring for the chelation of $Ca^{2+}_{(aq)}$ over $Mg^{2+}_{(aq)}$
430 will ensure that water in the immediate microenvironment of the EPS will have a lower
431 $(Mg/Ca)_{solution}$ than that of the bulk water and the water held within the biofilm matrix which
432 is not in the immediate microenvironment of the EPS molecules. Although it has been shown
433 that chelation exhibits an overall selectivity across a full biofilm based on charge density
434 (Rogerson *et al.*, 2008) it has also been demonstrated that some anionic groups differ in their
435 chelation affinities for Ca^{2+} and Mg^{2+} with some favouring calcium over magnesium and vice
436 versa (Table 3) (Wang *et al.*, 2009).

437 The complexity of these interactions would suggest that these influences would be rather
438 unpredictable and “noisy”, but we find a rather well organised relationship between
439 precipitation rate and $\text{Mg}/\text{Ca}_{(\text{calcite})}$. We propose that the very high calcium contents exhibited
440 at high precipitation rate is most likely to arise from utilisation of the metal pool chelated to
441 the EPS molecules (dominated by Ca^{2+} due to chemoselectivity). The bound cations may
442 form either unidentate or bidentate bonds with anionic functional groups on the EPS
443 molecules. Bidentate bonds form when both positive charges on the $\text{Ca}^{2+}_{(\text{aq})}$ are linked to
444 anionic groups, forming bidentate bridges between EPS molecules (Geesey and Yang, 1989).
445 Such an arrangement would be an inhibiting factor to calcite precipitation as free Ca^{2+} ions
446 have been removed from solution reducing the saturation index with respect to calcite
447 (Kawaguchi and Decho, 2002). However, if only one of the positive charges on a $\text{Ca}^{2+}_{(\text{aq})}$
448 cation is complexed with an anion (unidentate bonding) it leaves the other positive charge
449 free to bind with a CO_3^{2-} ion and initiate CaCO_3 precipitation by providing a nucleation site
450 for further precipitation (Shiraishi *et al.*, 2008, Decho, 2010). A further mechanism by which
451 $\text{Mg}/\text{Ca}_{(\text{calcite})}$ ratios may be reduced from expectation is through the incorporation unidentate
452 Ca^{2+} - ligand complexes into the precipitating solid. Figure 6 provides a schematic illustration
453 of unidentate/bidentate bonding and how nucleation sites may develop on the free positive
454 charge of a unidentate bonded Ca^{2+} .

455 **5 Conclusion**

456 The experimental results indicate that microbial metabolism and/or the presence of EPS
457 molecules overrides the expected thermodynamic control on $\text{Mg}/\text{Ca}_{(\text{calcite})}$ in ambient
458 temperature freshwater carbonate deposits. This was observed in both the flow through
459 microcosm and agitated flask precipitates. A significant relationship was found between
460 $(\text{Mg}/\text{Ca})_{\text{calcite}}$ ratios and precipitation rate for both the microcosm and agitated flask
461 experiments.

462 It has previously been reported that EPS preferentially chelates Ca^{2+} over Mg^{2+} resulting in
463 the microenvironment around the EPS molecules being enriched in calcium over magnesium
464 generating low $(\text{Mg}/\text{Ca})_{\text{calcite}}$ compared to that expected from the bulk water $(\text{Mg}/\text{Ca})_{\text{solution}}$
465 ratio (Rogerson *et al.*, 2008). This chemoselectivity favours the formation of Ca^{2+} - ligand
466 complexes, and the incorporation of some of these complexes into the precipitating solid will
467 both decrease precipitation activation energy (via “gel templating”) (Decho, 2010) and drive
468 the $(\text{Mg}/\text{Ca})_{\text{calcite}}$ ratio down from that expected from the bulk water $(\text{Mg}/\text{Ca})_{\text{solution}}$ ratio at a

469 given temperature. Our data implies that this process is fundamental in controlling the trace
470 element geochemistry of tufa carbonate.

471 Although several calibrations of the Mg/Ca palaeothermometer have been constructed for
472 foraminiferal and coralline calcite the findings here strongly suggest that the calibration of a
473 palaeothermometer is not a realistic prospect for tufa carbonates precipitated in the presence
474 of microbial biofilms. The finding that metal inclusion into precipitated calcite is accentuated
475 at low precipitation rates, and that the specific bonding character of cations and EPS
476 molecules are the primary regulator of this relationship, has impact well beyond
477 palaeothermometry. Generally, geoengineering practices where pollutants are extracted from
478 solution into carbonates aim at acceleration of the precipitation process. Our finding is that
479 this may always not be appropriate.

480 **6. Acknowledgements**

481 This research was supported by a University of Hull 80th Anniversary PhD scholarship. Mark
482 Anderson and Mike Dennett are thanked for their technical assistance and for assisting in the
483 running of the experiments. Tony Sinclair and Bob Knight are thanked for their assistance in
484 running the SEM and ICP – OES instruments respectively.

485 **7. References**

- 486
487 Anand, P., Elderfield, H., Conte, M.H. (2003) Calibration of Mg/Ca thermometry in
488 planktonic foraminifera from sediment trap time series. *Paleoceanography*, **18** (2), 1050.
- 489
490 Beer, T. (1996) *Environmental Oceanography*. CRC Press, Florida.
- 491
492 Benzerara, K., Menguy, N., Lopez-Garcia, P., Yoon, T.-H., Kazmierczak, J., Tyliszczak, T.,
493 Guyot, F. & Brown, G. E., Jr. 2006. Nanoscale detection of organic signatures in carbonate
494 microbialites. *Proceedings of the National Academy of Sciences* **103**, 9440-9445.
- 495
496 Bhaskar PV, Bhosle NB (2006) Bacterial extracellular polymeric substance (EPS): a carrier
497 of heavy metals in the marine food chain. *Environment International*, **32**, 191–198.
- 498
499 Bissett, A., Reimer, A., de Beer, D., Shiraishi, F. and Arp, G., (2008) Metabolic
500 microenvironmental control by photosynthetic biofilms under changing macroenvironmental
501 temperature and pH conditions. *Applied Environmental Microbiology*, **74**(20), 6306-6312.
- 502
503 Blanchard, G.F, Guarini, J.M, Richard, P., Gros, P., Mornet, F. (1996) Quantifying the short-
504 term temperature effect on lightsaturated photosynthesis on intertidal microphytobenthos.
505 *Marine Ecology Progress Series*, **134**, 309–313.

506
507 Boussetta, S., Bassinot, F., Sabbatini, A., Caillon, N., Nouet, J., Kallel, N., Rebaubier, H.,
508 Klinkhammer, G., Labeyrie, L. (2011) Diagenetic Mg-rich calcite in Mediterranean
509 sediments: Quantification and impact on foraminiferal Mg/Ca thermometry. *Marine Geology*,
510 **280 (1–4)**, 195–204.

511
512 Brasier, A.T., Andrews, J.E., Marca-Bell, A.D., Dennis, P.F. (2010) Depositional continuity
513 of seasonally laminated tufas: Implications for $\delta^{18}\text{O}$ based palaeotemperatures. *Global and*
514 *Planetary change*, **71 (3-4)**160 – 167.

515
516 Cacchio P, Ercole C, Cappuccio G, Lepidi A. (2003) Calcium carbonate precipitation by
517 bacterial strains isolated from limestone cave and from a loamy soil. *Geomicrobiology*
518 *Journal*, **20**, 85–98.

519
520 Cacchio P., Contento R., Ercole C., Cappuccio G., Martinez M. P. and Lepidi A. (2004)
521 Involvement of microorganisms in the formation of carbonate speleothems in the Cervo Cave
522 (L'Aquila—Italy). *Geomicrobiology Journal*, **21**, 497–509.

523
524 Chafetz, H., Rush, P.F. and Utech, N.M. (1991) Microenvironmental controls on mineralogy
525 and habit of CaCO precipitates: an example from an active travertine system. *Sedimentology*,
526 **38**, 107-126

527
528 Chave, K.E. (1954) Aspects of the biogeochemistry of magnesium: Calcareous marine
529 organisms. *Journal of Geology*, **62**. 266–283.

530
531 Couradeau, E., Benzerara, K., Gérard, E., Estève, I., Moreira, D., Tavera, R. & López-García,
532 P. 2013. Cyanobacterial calcification in modern microbialites at the submicrometer scale.
533 *Biogeosciences*, **10**, 5255-5266.

534
535 Decho, AW. (2000) Microbial biofilms in intertidal systems: an overview. *Continental Shelf*
536 *Research*, **20**, 1257–1273.

537
538 Decho, A.W. (2010) Overview of biopolymer-induced mineralization: What goes on in
539 biofilms? *Ecological Engineering*, **36(2)**, 137-144.

540
541 Defew, E. C., Perkins, R. G., Paterson, D. M. (2004) The influence of light and temperature
542 interactions on a natural estuarine microphytobenthic assemblage. *Biofilms*, **1**, 21–30.

543
544 Delaney, M.L., Be, A.W.H. and Boyle, E.A. (1985) Li, Sr, Mg and Na in foraminiferal calcite
545 shells from laboratory culture, sediment traps, and sediment cores. *Geochimica*
546 *Cosmochimica Acta*, **49**, 1327-1341.

547
548 Di Pippo, F.; Bohn, A.; Congestri, R.; De Philippis, R.; Albertano, P. Capsular
549 polysaccharides of cultured phototrophic biofilms. *Biofouling*, **25**, 495-504

550
551 Dittrich, M., Muller, B., Mavrocordatos, D. and Wehrli, B., 2003. Induced calcite
552 precipitation by cyanobacterium *Synechococcus*. *Acta Hydrochimica Et Hydrobiologica*,

553 **31(2)**, 162-169.

554

555 Dittrich, M. and Sibling, S. (2010) Calcium carbonate precipitation by cyanobacterial
556 polysaccharides. In: H.M. Pedley and M. Rogerson (Editors), *Speleothems and Tufas:
557 Unravelling Physical and Biological controls*. Geological Society Special Publication.
558 Geological Society of London, London, **336**, pp. 65-81.

559

560 Dupraz, C., Reid, P.R., Braissant, O., Decho, A.W. Norman, S.R. and Visscher, P.T. (2009).
561 Processes of carbonate precipitation in modern microbial mats. *Earth Science Reviews*, **96(3)**
562 141-162.

563

564 Elderfield, H., Bertram, C.J. and Erez, J. (1996) Biomineralization model for the
565 incorporation of trace elements into foraminiferal calcium carbonate, *Earth and Planetary
566 Science Letters*, **142**, 409–423.

567

568 Fairchild, I.J. and Treble, P.C. (2009) Trace elements in speleothems as recorders of
569 environmental change. *Quaternary Science Reviews*, **28**, 449–468

570

571 Garnett, E.R., Andrews, J.E., Preece, R.C., Dennis, P.F. (2004). Climatic change recorded by
572 stable isotopes and trace elements in a British Holocene tufa. *Journal of Quaternary Science*,
573 **19**, 251–262.

574

575 Geesey, G.G., Jang, L. (1989) Interactions between metal ions and capsular polymers. In:
576 Beveridge, T.J., Doyle, R.J. (Eds.), *Metal ions and bacteria*. Wiley, New York, pp. 325–357.

577

578 Hancke, K. and Glud, R.N. (2004) Temperature effects on respiration and photosynthesis in
579 three diatom-dominated benthic communities. *Aquatic Microbial Ecology*, **37**, 265-281.

580

581 Ihlenfeld C., Norman M., Gagan M., Drysdale R., Maas R. and Webb J. (2003) Climatic
582 significance of seasonal trace element and stable isotope variations in a modern freshwater
583 tufa. *Geochimica et Cosmochimica Acta*, **67**, 2341–2357

584

585 Kawaguchi, T. and Decho, A.W. (2002) Isolation and biochemical characterization of
586 extracellular polymeric secretions (EPS) from modern soft marine stromatolites (Bahamas)
587 and its inhibitory effect on CaCO₃ precipitation. *Biochemistry and Biotechnology*, **32**, 51–63.

588

589 Konhauser, K. (2007) *Introduction to Geomicrobiology*. Blackwell Publishing, Oxford.

590

591 Kısakürek, B., Eisenhauer, A., Böhm, F., Garbe-Schönberg, D. and Erez, J. (2008) Controls
592 on shell Mg/Ca and Sr/Ca in cultured planktonic foraminiferan, *Globigerinoides ruber*
593 (white). *Earth and Planetary Science Letters*, **273**, 260–269.

594

595 Lojen, S., Trkov, A., Ščančar, J., Vázquez-Navarro, Y.A. and Cukrov, N. (2009) Continuous
596 60-year stable isotopic and earth-alkali element records in a modern laminated tufa (Jaruga,
597 river Krka, Croatia): Implications for climate reconstruction. *Chemical Geology*, **258**, 242–

598 250.

599

600 Lorens, R. B. (1981) Sr, Cd, Mn and Co distribution coefficients in calcite as a function of
601 calcite precipitation rate. *Geochimica et Cosmochimica Acta*, **45**, 553–561.

602

603 Martínez-Botí, M.A., Mortyn, P.G., Schmidt, D.N., Vance, D., Field, D.B. (2011) Mg/Ca in
604 foraminifera from plankton tows: Evaluation of proxy controls and comparison with core
605 tops. *Earth and Planetary Science Letters*, **307**, 113-125.

606

607 Mitsuguchi, T., Matsumoto, E., Abe, O., Uchida, T., Isdale, P.J., (1996) Mg/Ca thermometry
608 in coral skeletons. *Science*, **274**, 961–963.

609

610 Morse, J. W. and Bender, M. L. (1990) Partition coefficients in calcite: Examination of
611 factors influencing the validity of experimental results and their application to natural
612 systems. *Chemical Geology* **82**, 265–277.

613

614 Morse, J.W. and Mackenzie, F.T. (1990) *Geochemistry of Sedimentary Carbonates*
615 (*Developments in Sedimentology*). Elsevier Science, London.

616

617 Mucci, A. (1987) Influence of temperature on the composition of magnesian calcite
618 overgrowths precipitated from seawater. *Geochimica et Cosmochimica Acta*, **51**, 1977-1984.

619

620 Nurnberg, D., Bijma, D. and Hemleben, C. (1996) .Assessing the reliability of magnesium in
621 foraminiferal calcite as a proxy for water mass temperatures, *Geochimica et Cosmochimica*
622 *Acta*, **60**, 803– 814.

623

624 Oomori T., Kaneshima H., and Maezato Y. (1987) Distribution coefficient of Mg²⁺ ions
625 between calcite and solution at 10–50°C. *Marine Chemistry* **20**, 327–336.

626

627 Pedley, H. M., Rogerson, M. and Middleton R. (2009) The growth and morphology of
628 freshwater calcite precipitates from in vitro mesocosm flume experiments. *Sedimentology*,
629 **56**, 511 – 527.

630

631 Pingitore, N.E., Eastmen, M.P., Sandidge, M., Oden, K., and Freiha, B. (1988) The
632 coprecipitation of manganese (II) with calcite: An experimental study. *Marine Chemistry*, **25**,
633 107–120.

634

635 Reynaud, S., Ferrier-Pages, C., Meibom, A., Mostefaoui, S., Mortlock, R., Fairbanks, R. and
636 Allemand, D. (2007) Light and temperature effects on Sr/Ca and Mg/Ca ratios in the
scleractinian coral *Acropora* sp. *Geochimica et Cosmochimica Acta*, **71**, 354 – 362.

637

638 Rimstidt J. D., Balog A., and Webb J. (1998) Distribution of trace elements between
639 carbonate minerals and aqueous solutions. *Geochimica et Cosmochimica Acta* **62**, 1851–
640 1863.

641

642 Rogerson, M., Pedley, H.M., Wadhawan, J.D. and Middleton, R. (2008) New insights into
643 biological influence on the geochemistry of freshwater carbonate deposits. *Geochimica et*
644 *Cosmochimica Acta*, **72**, 4976 – 4982.

645

646 Rogerson, M., Pedley, H.M., and Middleton, R. (2010) Microbial influence on
647 macroenvironment chemical conditions in alkaline (tufa) streams: perspectives from *in vitro*
648 experiments. In: H.M. Pedley and M. Rogerson (Editors), *Speleothems and Tufas:
649 Unravelling Physical and Biological controls*. Geological Society Special Publication
650 Geological Society of London, London, pp. 65-81.

651

652 Rosenthal, Y., Boyle, E.A. and Slowey, N. (1997) Environmental controls on the
653 incorporation of Mg, Sr, F and Cd into benthic foraminifera shells from Little Bahama Bank:
654 Prospects for thermocline paleoceanography. *Geochimica et Cosmochimica Acta*, **61**, 3633–
655 3643, 1997.

656

657 Salleh, S. and McMinn, A. (2011) The effects of temperature on the photosynthetic
658 parameters and recovery of two temperate benthic microalgae, amphora cf. coffeaeformis and
659 cocconeis cf. sublittoralis (bacillariophyceae). *Journal of Phycology*, **47**, 1413-1424.

660

661 Saunders, P.V., Moulin, F.Y., Eiff, O., Rogerson, M. (In press) Biofilms. In: L.E Frostick,
662 M.F. Johnson, R.E. Thomas, S.P. Rice and S.J. McLelland (Editors). *A Users Guide to
663 Ecohydraulic Experimentation*. IAHR book series, CRC Press, London.

664

665 Shirai K, Kusakabe M, Nakai S, Ishii T, Watanabe T, Hiyagon H, Sano Y. (2005) Deep-sea
666 coral geochemistry: implication for the vital effect. *Chemical Geology*, **224**, 212–222

667

668 Shiraishi, F., Bissett, A., de Beer, D., Reimer, A., Arp, G. (2008a) Photosynthesis, respiration
669 and exopolymer calcium-binding in biofilm calcification (Westerhöfer and Deinschwanger
670 Creek, Germany). *Geomicrobiology Journal*, **25**, 83–94.

671

672 Shiraishi, F., Okumura, T., Takahashi, Y., Kano, A., (2010) Influence of microbial
673 photosynthesis on tufa stromatolite formation and ambient water chemistry, SW Japan.
674 *Geochimica et Cosmochimica Acta*, **74**, 5289–5304.

675

676 Tesoriero, A. and Pankow, J. (1996) Solid solution partitioning of Sr^{2+} , Ba^{2+} , and Cd^{2+} to
677 calcite. *Geochimica et Cosmochimica Acta*, **60**, 1053–1063.

678

679 Wang, D.B., Wallace, A.F, De Yoreo, J.J., Dove, P.M. (2009) Carboxylated molecules
680 regulate magnesium content of amorphous calcium carbonates during calcification.
681 *Proceedings of National Academy of Sciences U.S.A.*, **106**, 21511–21516

682

683 Watermann F., Hillebrand, H., Gerdes, G., Krumbein, W.E., Sommer, U. (1999).
684 Competition between benthic cyanobacteria and diatoms as influenced by different grain
685 sizes and temperatures. *Marine Ecology Progress Series*, **187**, 77-87.

686

687 Wei, G., Sun, M., Li, X., Nie, B., (2000) Mg/Ca, Sr/Ca and U/Ca ratios of a porites coral
688 from Sanya Bay, Hainan Island, South China sea and their relationships to sea surface
689 temperature. *Palaeogeography Palaeoclimatology Palaeoecology*, **162**, 59–74.

690

691 Wolfaardt, G.M., Lawrence, J.R., Robarts, R.D., Caldwell, D.E. (1998) In situ
692 characterization of biofilm exopolymers involved in the accumulation of chlorinated
693 organics. *Microbiological Ecology*, **35**, 213–223.

694
695 Yoshimura, T., Tanimizu, M., Inoue, M., Suzuki, A., Iwasahi, N., Kawahata, H. (2011) Mg
696 isotope fractionation in biogenic carbonates of deep-sea coral, benthic foraminifera, and
697 hermatypic coral. *Analytical and bioanalytical chemistry*, **401(9)**, 2755 – 2769.

698
699 Yu, K.F., Zhao, J.X., Wei, G.J., Cheng, X.R., Chen, T.G., Felis, T., Wang, P.X., Liu, T.S.
700 (2006) $\delta^{18}\text{O}$, Sr/Ca and Mg/Ca records of *Porites lutea* corals from Leizhou Peninsula,
701 northern South China Sea, and their applicability as palaeoclimatic indicators.
702 *Palaeogeography, Palaeoclimatology, Palaeoecology*, **218**, 57–73.

703

704 Zhang, Y. and Dawe, R.A. (2000) Influence of Mg^{2+} on the kinetics of calcite precipitation
705 and calcite crystal morphology. *Chemical Geology*, **163**, 129-138.

706

707 Captions

708

709 Fig. 1. Schematic visualisation of the addition of the agitated 659 flask experiment to the microcosm
710 design. Arrows indicate direction of water flow.

711

712 Fig. 2. $(\text{Mg}/\text{Ca})_{\text{calcite}}$ ratios as a function of temperature: (a) Microcosms; (b) BFL; (c) BFD; (d)
713 Combined data. Error bars represent 1σ .

714

715 Fig. 3. Precipitation rate versus temperature. (a) Microcosms; (b) BFL; (c) BFD; (d) Combined data.

716

717 Fig. 4. $(\text{Mg}/\text{Ca})_{\text{calcite}}$ as a function of precipitation rate (a) Microcosms; (b) BFL; (c) BFD; (d) Combined
718 data.

719

720 Fig. 5. (a) Mean precipitation rates of all replicates from the microcosm, BFL and BFD experiments as
721 a function of temperature. (b) Mean precipitation rate as a function of temperature excluding the 20
722 °C data.

723

724 Fig. 6. Distribution coefficients as a function of precipitation rate from the microcosm and agitated
725 flask experiments combined.

726

727 Fig. 7. Schematic representation of unidentate and bidentate bonding of cations on anionic groups
728 of EPS molecules (represented by the two wavy lines). Nucleation sites are created on unidentate
729 bonded Ca_{2+} . The large arrows represent the continuous diffusion of ionic species into and out of
730 the microenvironment of the EPS molecules.

731

732 Table 1. Empirical and equilibrium distribution coefficients for selected divalent cations along with
733 ionic radii. The ionic radii are in six-fold coordination from Shannon and Prewitt, 1969. For reference
734 the ionic radii of Ca^{2+} is 1.00 (Table adapted from Rimstidt *et al.*, 1998).

735

736 Table 2. Binding constants for multicarboxylic acids. The Binding constant K is for the generalised
737 association reaction $\text{M}+\text{L} \rightleftharpoons \text{ML}$, with M representing the metal cation and L the ligand (adapted
738 from Wang *et al.*, 2009).

739

740

741 BENZERARA, K., MENGUY, N., LOPEZ-GARCIA, P., YOON, T.-H., KAZMIERCZAK, J., TYLISZCZAK, T.,
742 GUYOT, F. & BROWN, G. E., JR. 2006. Nanoscale detection of organic signatures in carbonate
743 microbialites. *Proceedings of the National Academy of Sciences* 103, 9440-9445.

744 COURADEAU, E., BENZERARA, K., GÉRARD, E., ESTÈVE, I., MOREIRA, D., TAVERA, R. & LÓPEZ-GARCÍA,
745 P. 2013. Cyanobacterial calcification in modern microbialites at the submicrometer scale.
746 *Biogeosciences*, 10, 5255-5266.

747 DECHO, A. W. 2010. Overview of biopolymer-induced mineralization: What goes on in biofilms?
748 *Ecological Engineering*, 36, 137-144.

749 PEDLEY, H. M., ROGERSON, M. & MIDDLETON, R. 2009. The growth and morphology of freshwater
750 calcite precipitates from in Vitro Mesocosm flume experiments; the case for biomediation.
751 *Sedimentology*, 56, , 511-527.

752 ROGERSON, M., PEDLEY, H. M., WADHAWAN, J. D. & MIDDLETON, R. 2008. New Insights into
753 Biological Influence on the Geochemistry of Freshwater Carbonate Deposits. *Geochimica et*
754 *Cosmochimica Acta*, 72, 4976-4987.

755

756

Table 1. Empirical and equilibrium distribution coefficients for selected divalent cations along with ionic radii. The ionic radii are in six-fold coordination from Shannon and Prewitt, 1969. For reference the ionic radii of Ca^{2+} is 1.00 (Table adapted from Rimstidt *et al.*, 1998).

Cation	Ionic radius	K_{exp}	K_{eq}
Ba^{2+}	1.36	0.020	1.95×10^{-2}
Cd^{2+}	0.95	188	6.92×10^3
Co^{2+}	0.65	10.9	4.68×10^1
Cu^{2+}	0.73	80.2	1.55×10^3
Fe^{2+}	0.61	27.7	2.40×10^2
Mg^{2+}	0.72	0.022	8.71×10^{-4}
Mn^{2+}	0.67	20.5	1.41×10^2
Pb^{2+}	1.18	17.2	2.63×10^3
Ra^{2+}	1.44	0.020	1.91×10^{-3}
Sr^{2+}	1.16	0.073	1.82×10^{-1}

Table 2. Mean precipitation rates from lowest to highest as related to experimental conditions.

Experiment type	Temperature (°C)	Precipitation rate ($\mu\text{mol cm}^{-2} \text{hr}^{-1}$)
Microcosm	12	0.027
Microcosm	14	0.047
Microcosm	16	0.007
Microcosm	18	0.065
Microcosm	12	0.027
BFL	12	0.012
BFL	14	0.107
BFL	16	0.113
BFL	18	0.023
BFL	20	0.177
BFD	12	0.006
BFD	14	0.056
BFD	16	0.034
BFD	18	0.036
BFD	20	0.116

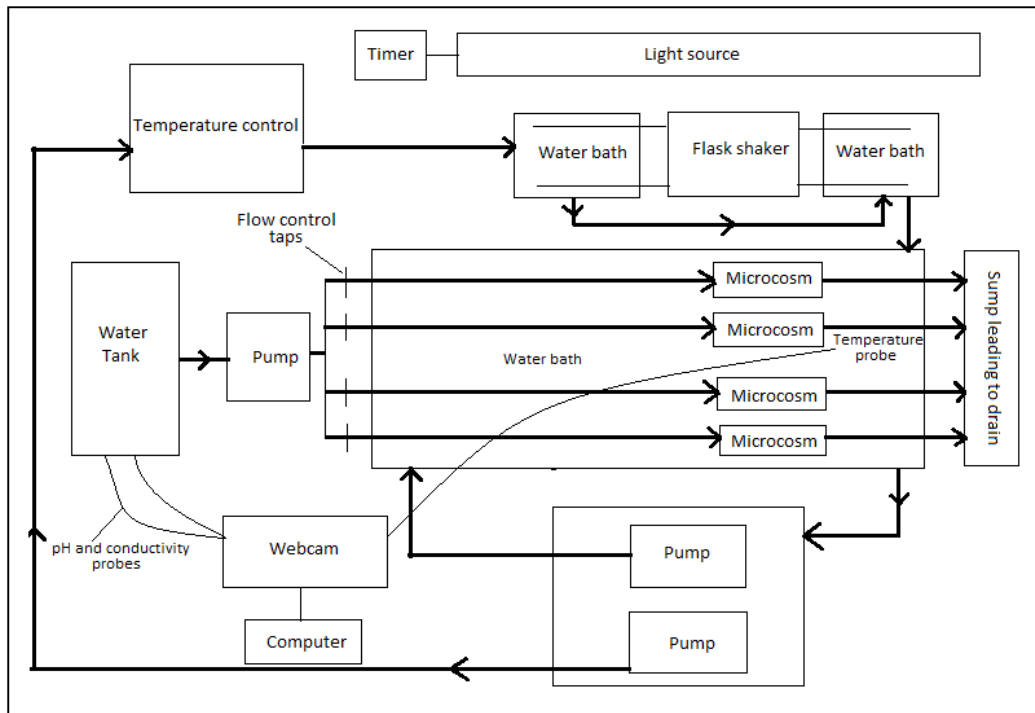


Figure 1. Schematic visualisation of the addition of the agitated flask experiment to the microcosm design. Arrows indicate direction of water flow.

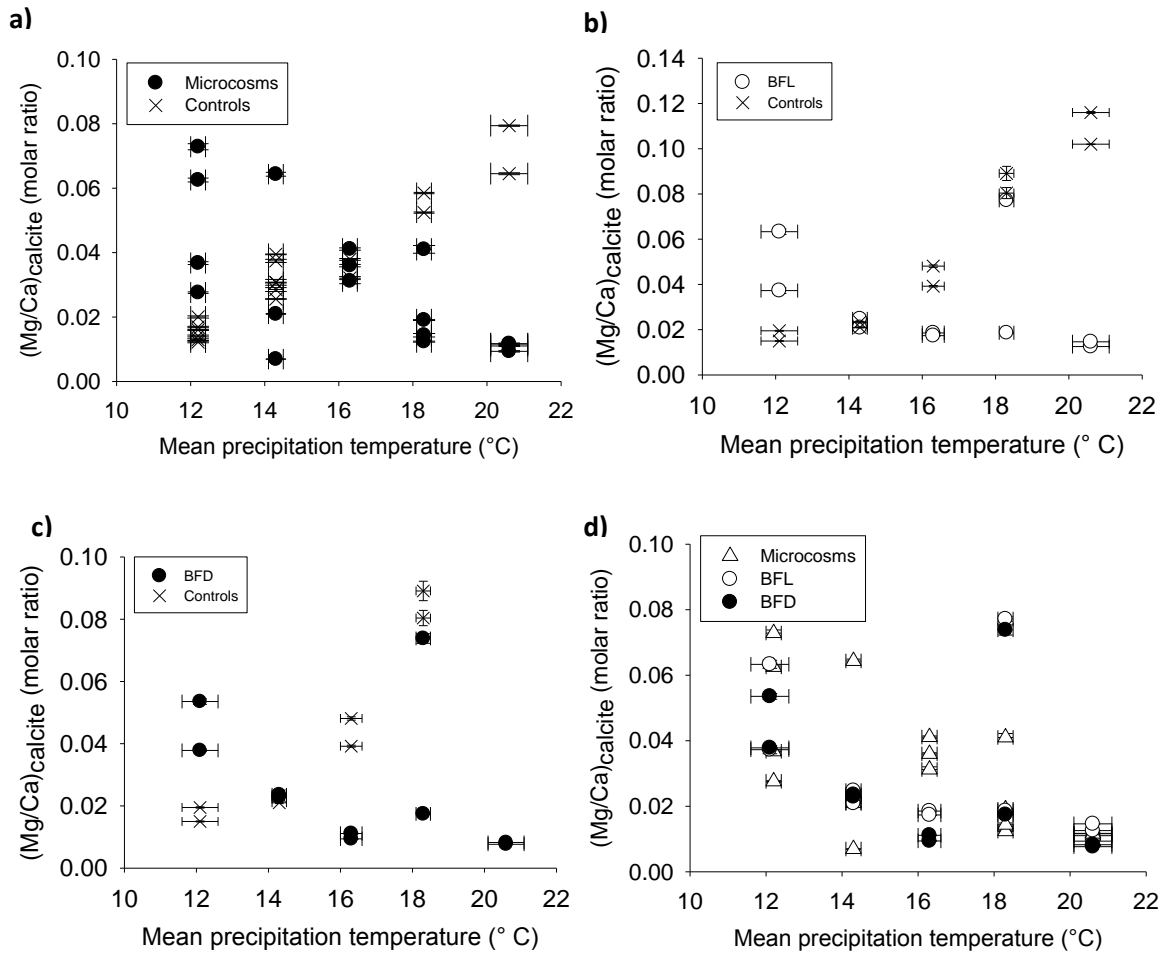


Figure 2. $(\text{Mg}/\text{Ca})_{\text{calcite}}$ ratios as a function of temperature: (a) Microcosms; (b) BFL; (c) BFD; (d) Combined data. Error bars represent 1σ .

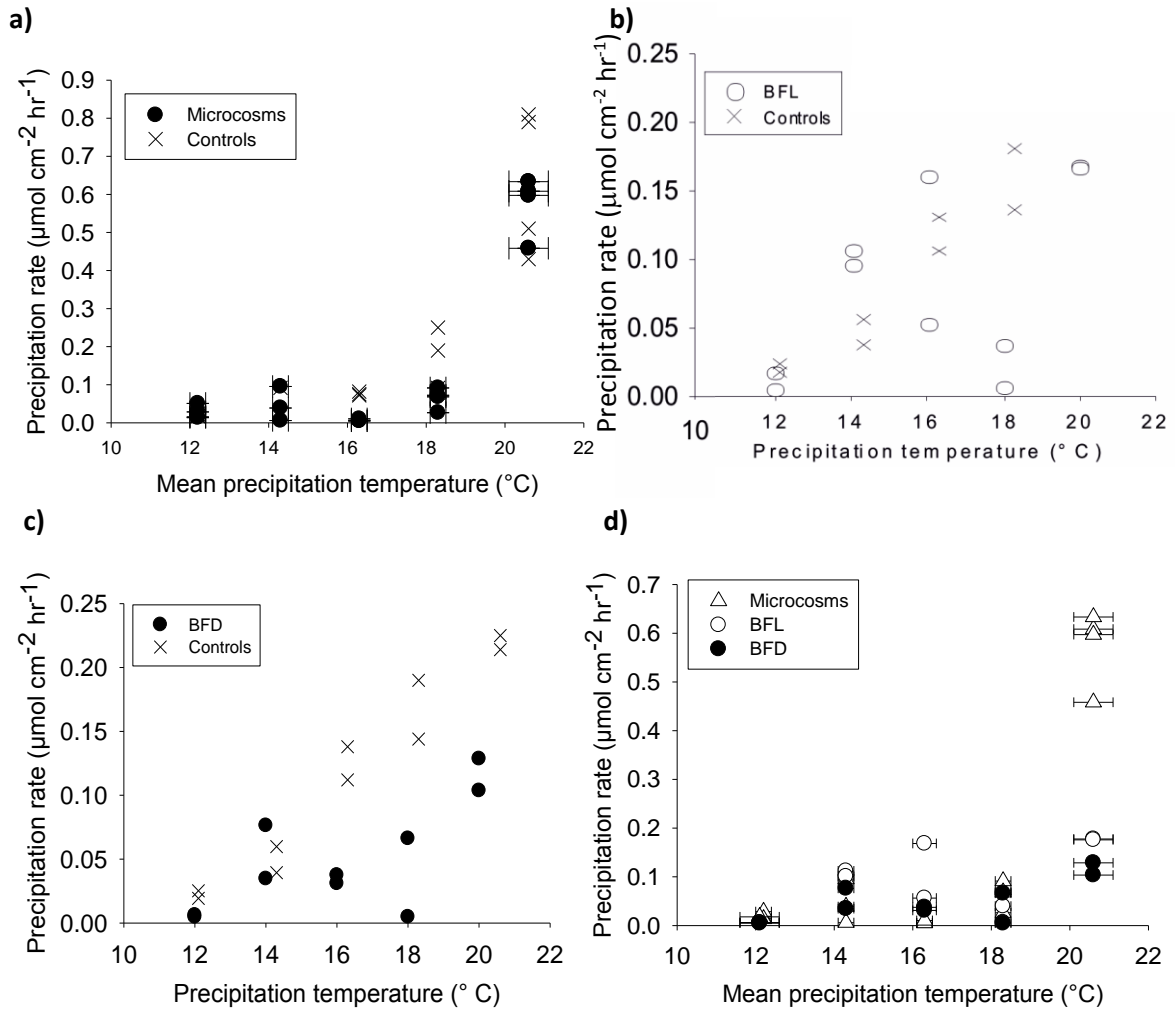


Fig. 3. Precipitation rate versus temperature. (a) Microcosms; (b) BFL; (c) BFD; (d) Combined data.

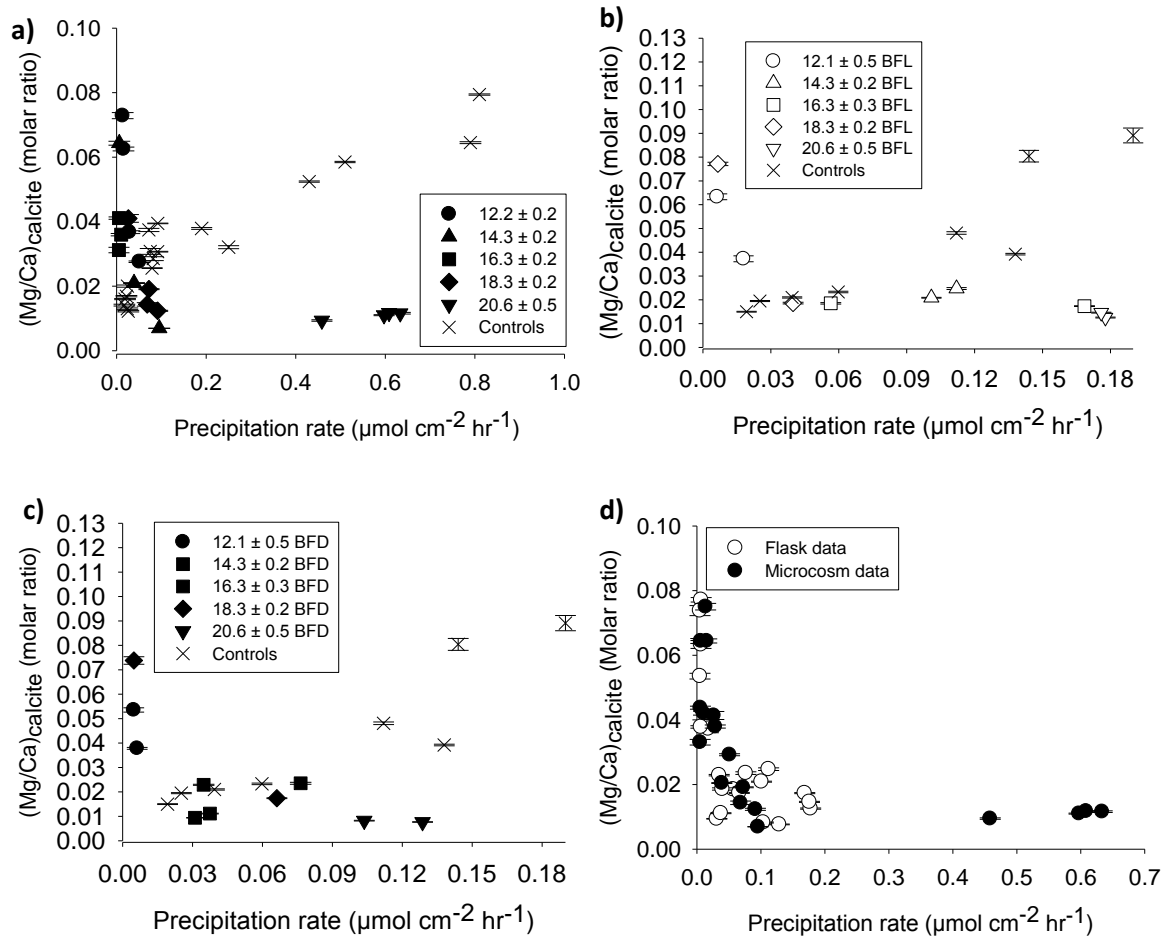


Figure 4. $(\text{Mg}/\text{Ca})_{\text{calcite}}$ as a function of precipitation rate (a) Microcosms; (b) BFL; (c) BFD; (d) Combined data.

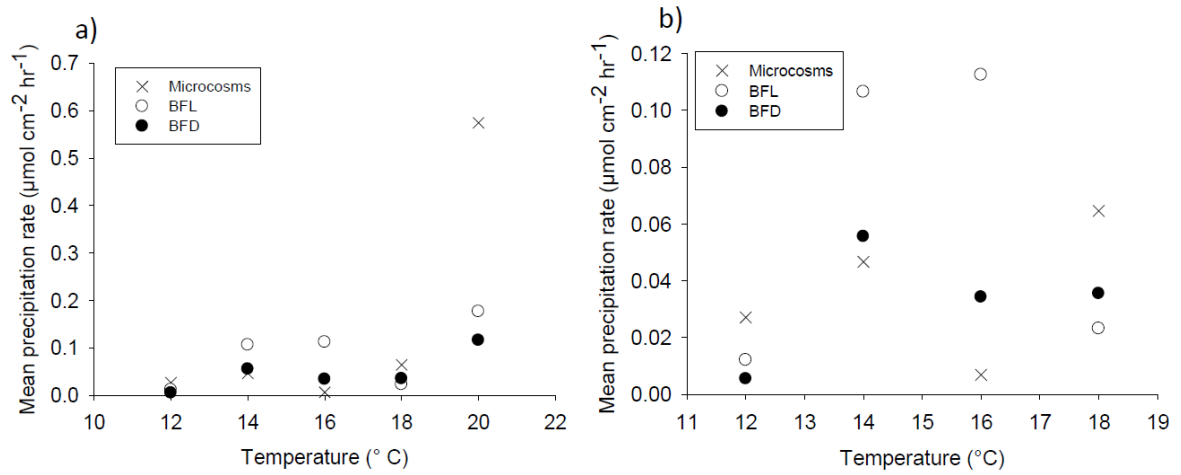


Fig. 5. (a) Mean precipitation rates of all replicates from the microcosm, BFL and BFD experiments as a function of temperature. (b) Mean precipitation rate as a function of temperature excluding the 20 $^{\circ}\text{C}$ data.

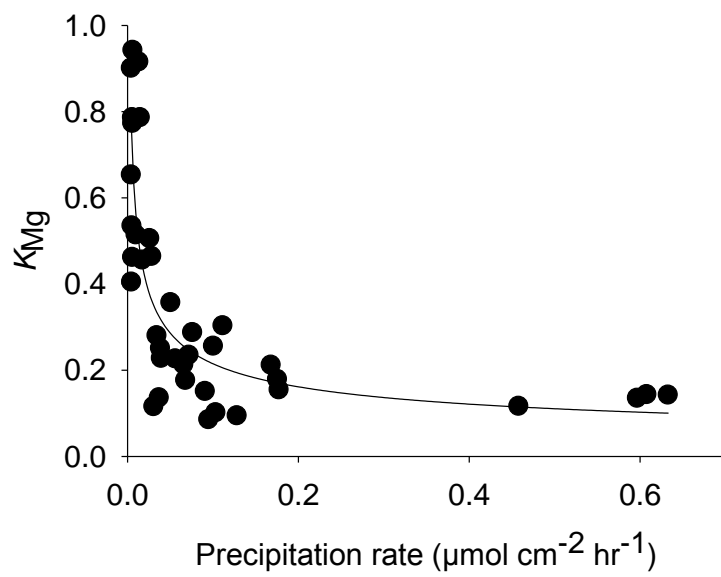


Figure 6. Distribution coefficients as a function of precipitation rate from the microcosm and agitated flask experiments combined.

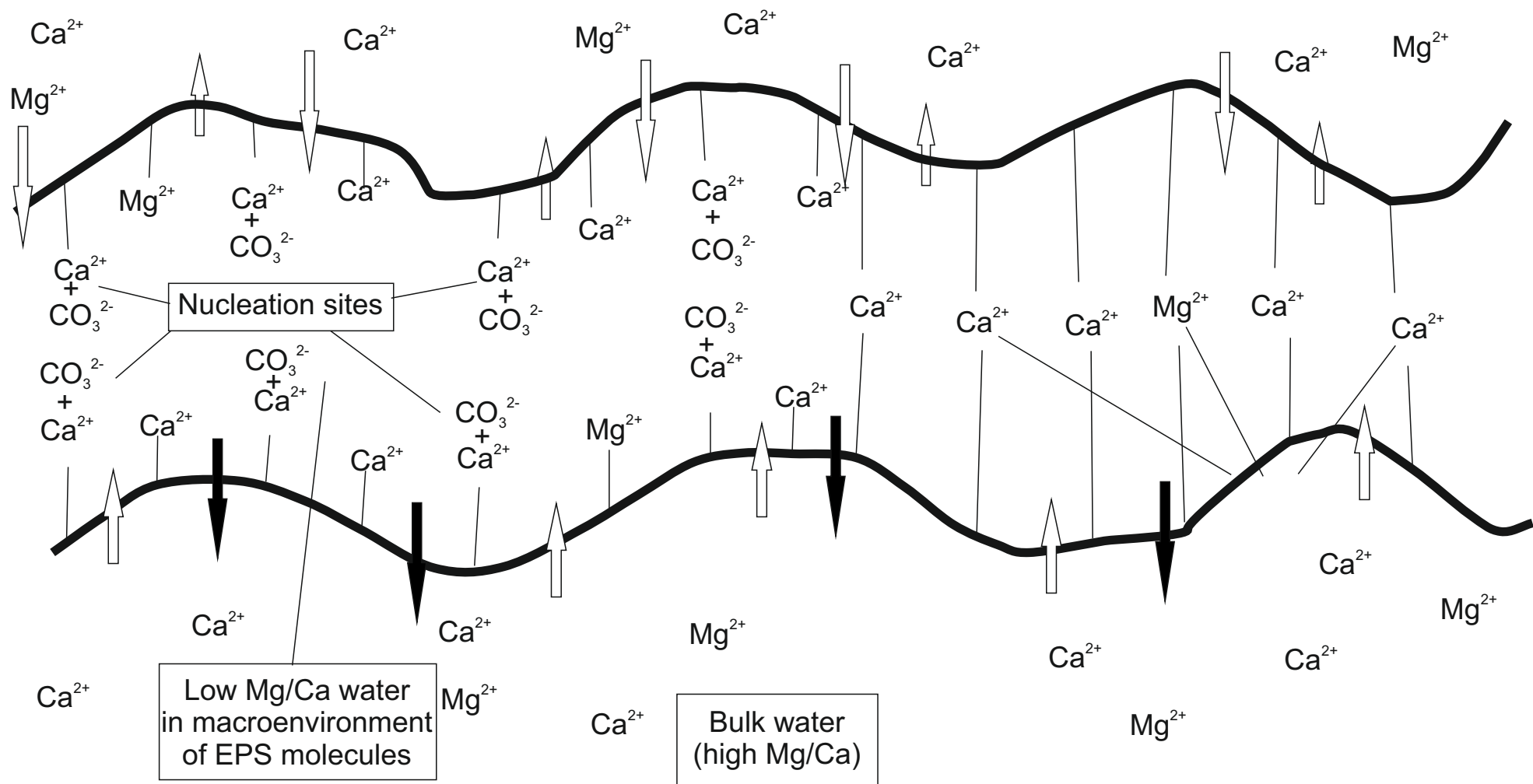


Fig. 7. Schematic representation of unidentate and bidentate bonding of cations on anionic groups of EPS molecules (represented by the two wavy lines). Nucleation sites are created on unidentate bonded Ca^{2+} . The large arrows represent the continuous diffusion of ionic species into and out of the microenvironment of the EPS molecules.